On-axis computer-generated holograms based on centrosymmetric partitioning of the pixel

Uriel Levy, Yoav Shrot, Emanuel Marom, and David Mendlovic

A novel, to our knowledge, configuration for the design and fabrication of zero-order computer-generated holograms in which each pixel is split into two centrosymmetric equal-sized regions is proposed and tested. In a manner similar to other approaches this configuration also permits the encoding and the reconstruction of a complex function that exhibits phase as well as amplitude variations by use of a phase-only filter. A detailed mathematical analysis is followed by evaluation of the error of the encoding approach, which is calculated and compared with the error exhibited by other approaches. Computer simulations as well as optical experiments demonstrate the capabilities of this novel configuration. © 2001 Optical Society of America

OCIS codes: 090.1970, 050.1380, 100.5090.

1. Introduction

Diffractive optical elements play a major role in various applications such as beam shaping,[1] optical data processing,[2] optical interconnections,[3] and imaging.[4] Many of those elements, which are required to generate a complex wave front, are calculated numerically. The computed function is then implemented either as an amplitude-only filter or as a phase-only filter. Proper encoding of such filters allows the generation of a complex (amplitude and phase) field as is necessary, for instance, for optical correlation applications for which the phase as well as the amplitude need to be accurately reconstructed.

Such elements have been coined computer-generated holograms (CGHs) and were first introduced by Lohmann *et al.*[5,6] The CGHs were implemented by use of a binary carrier (grating) and provided the desired complex-function distributions at arbitrary planes along the direction of a predefined off-axis diffraction order. Because the phase modulation was achieved by the shifting of a rectangular aperture within each pixel, the technique was called a detour phase CGH. This revolutionary approach was later followed by others so that several off-axis CGH-encoding methods were proposed.[7–11] A review of these approaches was given by Lee.[12] A common feature of all those methods is that the reconstructed image is displayed along a well-defined off-axis diffraction order, whereas the conjugate image is obtained along the opposite order. It is worth mentioning that it has recently[13] been shown that it is possible to obtain different desired reconstructions along two conjugated orders, provided that a Fresnel (rather than a Fourier) CGH is used.

A major disadvantage in generating an off-axis light-distribution presentation is the high sensitivity to wavelength variations. Wavelength broadening increases the blurring effect and thus reduces the reconstruction quality. Wavelength deviation shifts the position of the expected reconstruction, and in the case of the phase-carrier grating it also reduces the diffraction efficiency. Moreover, off-axis reconstruction increases the complexity of the system owing to the alignment requirements, which are more intricate compared with those for on-axis systems.

Because on-axis reconstruction seems to be advantageous in some aspects compared with off-axis reconstruction, zero-order encoding methods become highly desirable. As a result of significant developments in microelectronics and micro-optics fabrication capabilities, the fact that zero-order encoding methods require multilevel phase structures is no longer a deterring factor. Several zero-order encoding methods[14–17] have been already suggested. Unfortunately, these approaches require high spatial resolution to achieve a reasonable number of gray levels. One may trade the demand for high spatial

The authors are with the Faculty of Engineering, Tel-Aviv University, 69978 Tel-Aviv, Israel. D. Mendlovic's e-mail address is mend@eng.tau.ac.il.

Received 26 January 2001; revised manuscript received 19 April 2001.
0003-6935/01/325928-10$15.00/0

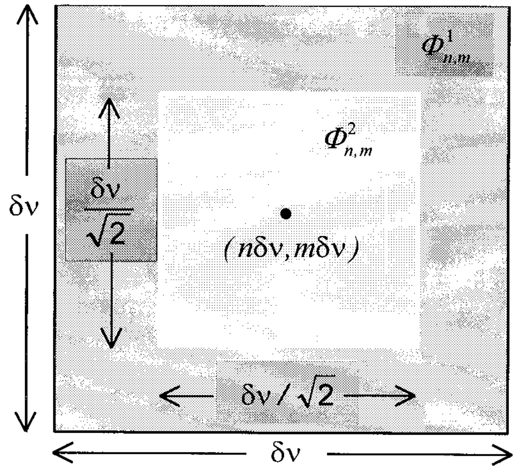

Fig. 1. Basic macropixel cell configurations.

resolution for the requirement of high etching resolution by using an approach based on the fixed spatial partitioning of the pixels.[18,19] The reconstruction achieved with the above approach suffers from significant degradation that is due to the nonsymmetric structure of the CGH, which leads to a pseudo, undesired detour phase effect. By dividing each pixel into a 4×4 pixel symmetric structure, one obtains an improvement that significantly reduces the reconstruction error.[19] Nevertheless, such improvement was achieved because of higher fabrication requirements.

In the following, we present a simplified encoding method that is based on partitioning each pixel into two centrosymmetric subregions wherein each of them requires different phase values (different etching levels). The symmetric structure not only reduces reconstruction error but also allows ease of comparison with other approaches. Because each region is continuous, mask generation is less demanding, and the etching process becomes simpler. Mathematical analysis of this approach is given in Section 2. Error estimation and performance evaluations are discussed in Section 3, whereas in Section 4 the suggested approach is compared with other encoding methods. Computer simulations are detailed in Section 5, and Section 6 describes the optical experiment. Conclusions given in Section 7 complete this paper.

2. Encoding Procedure

As was suggested earlier by Florence and Juday,[18] the proposed configuration is also based on dividing each pixel (coined a macropixel) into two subpixels with equal area. For each of these subpixels a specific phase value is allocated and etched so that a predetermined phase value and a normalized amplitude of the macropixel is obtained, as is shown below. The purpose of the subdivision is the encoding of phase and amplitude information through phase-only variations in the filter. The innovation of the suggested novel configuration is based on the centrosymmetric partitioning of the pixels, i.e., achieving two subregions with a common center. This configuration is expected to reduce the reconstruction error because the common center should avoid any undesired phase shift between the two subregions.

A two-dimensional (2-D) top view of a basic macropixel is illustrated in Fig. 1. The two free parameters shown, $\phi^1_{n,m}$ and $\phi^2_{n,m}$, are the phases etched in each one of the two partitions of the basic cell. The filter is mathematically described by

$$H(\nu_x, \nu_y) = \sum_n \sum_m H_{n,m}, \tag{1}$$

where $H_{n,m}$ is the transfer function of a single macropixel and is calculated in accord with

$$\begin{aligned} H_{n,m}(\nu_x, \nu_y) = \Bigg\{ \Bigg[& \mathrm{rect}\left(\frac{\nu_x}{\delta\nu_x}, \frac{\nu_y}{\delta\nu_y}\right) \\ & - \mathrm{rect}\left(\frac{\nu_x}{\frac{\delta\nu_x}{\sqrt{2}}}, \frac{\nu_y}{\frac{\delta\nu_y}{\sqrt{2}}}\right)\Bigg] \exp(i\phi^1_{n,m}) \\ & + \left[\mathrm{rect}\left(\frac{\nu_x}{\frac{\delta\nu_x}{\sqrt{2}}}, \frac{\nu_y}{\frac{\delta\nu_y}{\sqrt{2}}}\right)\right] \exp(i\phi^2_{n,m}) \Bigg\} \\ & * \delta(\nu_x - n\delta\nu, \nu_y - m\delta\nu). \end{aligned} \tag{2}$$

Here the asterisk denotes convolution, $\delta\nu$ is the lateral dimension of the pixel, δ is the Dirac impulse function, and

$$\begin{aligned} \mathrm{rect}(\alpha, \beta) &= \mathrm{rect}(\alpha)\mathrm{rect}(\beta) \\ &= \begin{cases} 1 & -0.5 < \alpha, \beta < 0.5 \\ 0 & \text{elsewhere} \end{cases}. \end{aligned} \tag{3}$$

By taking $h(x, y)$ to be the inverse Fourier transform of $H(\nu_x, \nu_y)$, one obtains

$$h(x, y) = \int_{-\infty}^{\infty} \int_{-\infty}^{\infty} H(\nu_x, \nu_y) \exp[i2\pi(x\nu_x + y\nu_y)] \mathrm{d}\nu_x \mathrm{d}\nu_y. \tag{4}$$

Substituting Eq. (2) into Eq. (4) results in

$$\begin{aligned} h(x, y) = \delta\nu_x\delta\nu_y \sum_n \sum_m \Bigg\{ \Bigg[& \sin c(\delta\nu_x x) \sin c(\delta\nu_y y) \\ & - \frac{1}{2} \sin c\left(\frac{\delta\nu_x}{\sqrt{2}} x\right) \sin c\left(\frac{\delta\nu_y}{\sqrt{2}} y\right)\Bigg] \exp(i\phi^1_{n,m}) \\ & + \left[\frac{1}{2} \sin c\left(\frac{\delta\nu_x}{\sqrt{2}} x\right) \sin c\left(\frac{\delta\nu_y}{\sqrt{2}} y\right)\right] \\ & \times \exp(i\phi^2_{n,m}) \Bigg\} \exp[i2\pi(xn\delta\nu_x + ym\delta\nu_y)], \end{aligned} \tag{5}$$

where $\sin c(x)$ is defined as

$$\sin c(x) = \frac{\sin(\pi x)}{\pi x}. \quad (6)$$

Because this encoding method enables on-axis zero-order reconstruction, we restrict our attention to regions of (x, y) that correspond to $x \ll 1/\delta\nu_x$ and $y \ll 1/\delta\nu_y$. Consequently

$$x\delta\nu_x \ll 1, \qquad y\delta\nu_y \ll 1. \quad (7)$$

As a result all sinc expressions become asymptotically equal to 1:

$$\sin c(\delta\nu_x x),\ \sin c(\delta\nu_y y),\ \sin c\left(\frac{\delta\nu_x}{\sqrt{2}}x\right),\ \sin c\left(\frac{\delta\nu_y}{\sqrt{2}}y\right) \approx 1. \quad (8)$$

Substituting expressions (8) into Eq. (5) yields

$$h(x, y) = \frac{\delta\nu_x\delta\nu_y}{2}\sum_n\sum_m [\exp(i\phi^1_{n,m}) + \exp(i\phi^2_{n,m})] \times \exp[i2\pi(xn\delta\nu_x + ym\delta\nu_y)]. \quad (9)$$

In a discrete system the filter $H(\nu_x, \nu_y)$ should represent an arbitrary normalized complex distribution that, within a given macropixel (n, m), is given by

$$H(n\delta\nu_x, m\delta\nu_y) = A_{n,m}\exp(i\phi_{n,m}). \quad (10)$$

The Fourier integral of Eq. (4) is thus replaced with a summation:

$$h(x, y) \approx \delta\nu_x\delta\nu_y\sum_n\sum_m H(n\delta\nu_x, m\delta\nu_y) \times \exp[i2\pi(xn\delta\nu_x + ym\delta\nu_y)]. \quad (11)$$

The expression in the square brackets on the right-hand side of Eq. (9) can be manipulated mathematically to provide

$$h(x, y) = \delta\nu_x\delta\nu_y\sum_n\sum_m \cos\left(\frac{\phi^1_{n,m} - \phi^2_{n,m}}{2}\right) \times \exp\left(\frac{\phi^1_{n,m} + \phi^2_{n,m}}{2}\right)\exp[i2\pi(xn\delta\nu_x + ym\delta\nu_y)]. \quad (12)$$

One can readily see from Eq. (12) that the resulting amplitude and phase of each macropixel are uniquely determined by $\phi^1_{n,m}$ and $\phi^2_{n,m}$, according to

$$A_{n,m} = \cos\left(\frac{\phi^1_{n,m} - \phi^2_{n,m}}{2}\right), \quad (13)$$

$$\phi_{n,m} = \frac{\phi^1_{n,m} + \phi^2_{n,m}}{2}, \quad (14)$$

respectively. One can readily see from Eq. (13) that $A_{n,m} \leq 1$ is determined uniquely by the difference in the values of $\phi^1_{n,m}$ and $\phi^2_{n,m}$. The term $(1 - A_{n,m})$ represents the light that is diverted to areas outside the region of interest. Hence if the samples of the Fourier transform of the desired image are given by the discrete values $H(n\delta\nu_x, m\delta\nu_y)$, as defined by Eq. (10), then $\phi^1_{n,m}$ and $\phi^2_{n,m}$ are uniquely determined to be

$$\phi^1_{n,m} = \phi_{n,m} + \cos^{-1}(A_{n,m}), \quad (15)$$

$$\phi^2_{n,m} = \phi_{n,m} - \cos^{-1}(A_{n,m}). \quad (16)$$

Thus a phase-only filter can encode amplitude as well as phase.

3. Error Estimation

The proposed approach is based on the approximations presented in expressions (8). However, these approximations result in some error, hence in some performance reduction. The main drawback of the encoding procedure lies in the fact that each subpixel does not have an infinitesimal size but rather finite dimensions. The sources of error are associated with the different combinations of sinc products multiplying the phase terms in Eq. (5), namely,

$$\left[\frac{1}{2}\sin c\left(\frac{\delta\nu_x}{\sqrt{2}}x\right)\sin c\left(\frac{\delta\nu_y}{\sqrt{2}}y\right)\right],$$

$$\left[\sin c(\delta\nu_x x)\sin c(\delta\nu_y y) - \frac{1}{2}\sin c\left(\frac{\delta\nu_x}{\sqrt{2}}x\right)\sin c\left(\frac{\delta\nu_y}{\sqrt{2}}y\right)\right].$$

Because each term in the argument of summation is multiplied by a different complex number $[\exp(i\phi^1_{n,m})$ or $\exp(i\phi^2_{n,m})]$, every point (x, y) of the whole reconstructed plane is influenced differently and cannot be precompensated.

To evaluate the significance of the error, let us analyze a specific example. If a certain pixel, say, (n, m), should represent values of $A_{n,m} = 0.5$ and $\phi_{n,m} = 0$, according to the proposed encoding method [Eqs. (15) and (16)], the phase values of the subpixels should be set to $\phi^1_{n,m} = \pi/3$ and $\phi^2_{n,m} = -\pi/3$. The reconstructed object $h(x, y)$ is confined to the region (x, y) that satisfies $|x|\delta\nu_x \leq 1/2$, $|y|\delta\nu_y \leq 1/2$. If one takes into account the additional sinc terms and calculates from these phase values the amplitude and the phase it can be seen that, at the center of the reconstruction region $(x, y = 0)$, the expected result is indeed unchanged: $\phi_{n,m} = 0$ and $A_{n,m} = 0.5$. However, when examining the edges $(x = \pm 1/2\delta\nu_x, y = 0)$ the obtained values are $A_{n,m} = 0.35$ and $\phi_{n,m} = -0.138\pi$, which, compared with the values at the center, represent large errors.

For improving the performance and minimizing the effect of the error terms the use of zero padding, namely, surrounding the original object with zeros, is recommended. This approach is equivalent to reducing the incremental frequency step $\delta\nu$ in the Fourier transform plane. Let the original object size be $u_{\max}$; the added strip of zeros then increases it to $U_{\max}$. The new incremental frequency step $\delta\nu$ is $1/U_{\max}$. The size ratio is defined as

$$P = \frac{U_{\max}}{u_{\max}}. \quad (17)$$

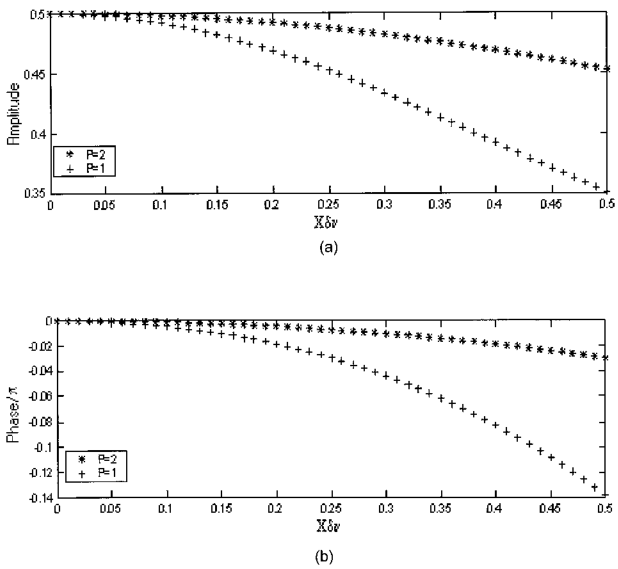

Fig. 2. Deviations from the desired complex value within the cell of interest along the horizontal axis: (a) amplitude deviations, (b) phase deviations. Results are plotted for input with padding ($P = 2$) of the same size as the object and without padding ($P = 1$).

The reconstructed image will indeed have a size $U_{\max}$; however, the region of interest is restricted to $|X| \leq u_{\max}/2 = 1/(2\delta\nu P)$, and thus the approximation of expressions (7) is better satisfied. Assuming, for instance, that $P = 2$ and using the previous example show that the values obtained are $A_{n,m} = 0.452$ and $\phi_{n,m} = -0.03\pi$, which are significant improvements in both phase and amplitude compared with the case of $P = 1$. The obtained amplitude and phase values for both $P = 1$ and $P = 2$ along the x axis are displayed in Figs. 2(a) and 2(b), respectively.

Table 1 provides a summary of the expected performance of the proposed approach that is based on the examination of three amplitude cases, $A_{n,m} = 0.5$, $A_{n,m} = 0.1$, and $A_{n,m} = 1$, and two phase cases, $\phi_{n,m} = 0.3\pi$ and $\phi_{n,m} = 1.5\pi$. The maximum deviation from these values (which occurs at the edges of the reconstructed image) was evaluated for $P = 1, 2, 4, 8, 16$. The important parameter in Table 1 is the relative-error parameter, defined as

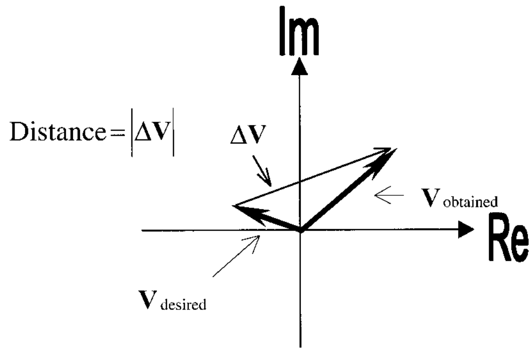

Fig. 3. Vector description of the distance function [Eq. (19)] between phasors.

$$\text{Percent error} = 100\,\frac{\text{Distance}}{A_{\text{desired}}}, \tag{18}$$

where the distance is the geometrical separation between the obtained and the desired phasor (Fig. 3):

$$\text{Distance} = [|A_{\text{obtained}}{}^2 + A_{\text{desired}}{}^2 - 2A_{\text{obtained}}A_{\text{desired}}\cos(\phi_{\text{obtained}} - \phi_{\text{desired}})|]^{1/2}. \tag{19}$$

It can be seen that, for all the amplitude values and when P is set to 16, the relative error is less than 1% (see the last row of Table 1). One must keep in mind that these relative-error values are the maximum deviation values possible, and thus the average values are much smaller. In fact, in the center of the

Table 1. Maximum-Error Evaluation for the Proposed Technique

		Maximum Error					
		$A_{\text{desired}} = 0.1$		$A_{\text{desired}} = 0.5$		$A_{\text{desired}} = 1$	
P	Obtained Measure	$\phi_d = 0.3\pi$	$\phi_d = 1.5\pi$	$\phi_d = 0.3\pi$	$\phi_d = 1.5\pi$	$\phi_d = 0.3\pi$	$\phi_d = 1.5\pi$
1	Amplitude	0.181	0.18	0.35	0.35	0.636	0.636
	Phase	-0.085π	1.11π	0.162π	1.36π	0.3π	1.5π
	Relative error	173%	173%	46.8%	46.8%	36%	36%
2	Amplitude	0.102	0.102	0.452	0.452	0.9	0.9
	Phase	0.141π	1.342π	0.27π	1.47π	0.3π	1.5π
	Relative error	50%	50%	13%	13%	10%	10%
4	Amplitude	0.098	0.098	0.487	0.487	0.974	0.974
	Phase	0.258π	1.458π	0.292π	1.492π	0.3π	1.5π
	Relative error	13%	12.9%	3.3%	3.3%	2.5%	2.5%
8	Amplitude	0.0994	0.0994	0.496	0.496	0.993	0.993
	Phase	0.289π	1.489π	0.298π	1.496π	0.3π	1.5π
	Relative error	3.25%	3.25%	0.8%	0.8%	0.6%	0.6%
16	Amplitude	0.0998	0.0998	0.499	0.499	0.998	0.998
	Phase	0.297π	1.497π	0.299π	1.499π	0.3π	1.5π
	Relative error	0.8%	0.8%	0.2%	0.2%	0.1%	0.1%

Table 2. Maximum-Error Evaluation for Ref. 19 (1-D Configuration)

		Maximum Error					
		$A_{desired} = 0.1$		$A_{desired} = 0.5$		$A_{desired} = 1$	
P	Obtained Measure	$\phi_d = 0.3\pi$	$\phi_d = 1.5\pi$	$\phi_d = 0.3\pi$	$\phi_d = 1.5\pi$	$\phi_d = 0.3\pi$	$\phi_d = 1.5\pi$
1	Amplitude	0.27	0.27	0.39	0.39	0.636	0.636
	Phase	-0.124π	1.07π	0.101π	1.3π	0.3π	1.5π
	Relative error	264%	164%	58.3%	58.3%	36%	36%
2	Amplitude	0.116	0.116	0.454	0.454	0.9	0.9
	Phase	0.08π	1.28π	0.254π	1.454π	0.3π	1.5π
	Relative error	74.5%	74.5%	16%	16%	10%	10%
4	Amplitude	0.099	0.099	0.487	0.487	0.974	0.974
	Phase	0.238π	1.438π	0.289π	1.489π	0.3π	1.5π
	Relative error	19%	19%	4.1%	4.1%	2.5%	2.5%
8	Amplitude	0.0994	0.0994	0.496	0.496	0.993	0.993
	Phase	0.284π	1.484π	0.297π	1.497π	0.3π	1.5π
	Relative error	4.82%	4.8%	1%	1%	0.6%	0.6%
16	Amplitude	0.0998	0.0998	0.499	0.499	0.998	0.998
	Phase	0.296π	1.496π	0.299π	1.499π	0.3π	1.5π
	Relative error	1.2%	1.2%	0.26%	0.26%	0.1%	0.1%

reconstruction region no error occurs. Because this CGH is based on far-field reconstruction, the significance of the phase information is very high. As can also be seen from Table 1, at high-amplitude levels the phase error is zero, thus avoiding significant errors in the reconstructed image. The low relative-error values of the new method result in high performance, as is demonstrated below.

4. Comparison of Various Hologram-Encoding Techniques

To evaluate the potential of the proposed method, we conducted a quantitative comparison with previous methods.[17,19] The comparison was based on the relative-error expression, according to Eq. (18). For the sake of proper comparison the obtained phase and amplitude as well as the relative error were calculated, based on the same test cases that were investigated in Section 3, for each of the previous approaches.

Results for the approach described in Ref. 19 (fixed partitions, variable phase levels) are given in Table 2. Table 3 presents the results obtained for the variable-partition, fixed-phase-level case.[17] It should be emphasized that Ref. 19 suggests three techniques: a basic approach (asymmetric partition), a one-dimensional (1-D) improved structure (symmetric partition), and 2-D improved structure (symmetry along both axes). The calculation of the relative error for this reference was based on the improved 1-D case because its performances were superior to those of the basic approach. The 2-D improved structure

Table 3. Maximum-Error Evaluation for Ref. 17

		Maximum Error					
		$A_{desired} = 0.1$		$A_{desired} = 0.5$		$A_{desired} = 1$	
P	Obtained Measure	$\phi_d = 0.3\pi$	$\phi_d = 1.5\pi$	$\phi_d = 0.3\pi$	$\phi_d = 1.5\pi$	$\phi_d = 0.3\pi$	$\phi_d = 1.5\pi$
1	Amplitude	0.296	0.381	0.236	0.766	CBE[a]	CBE
	Phase	-0.667π	1.41π	-0.596π	1.54π	CBE	CBE
	Relative error	396%	286%	145.6%	155%	CBE	CBE
2	Amplitude	0.112	0.264	0.137	0.7	CBE	CBE
	Phase	-0.52π	1.47π	0.208π	1.544π	CBE	CBE
	Relative error	204%	164%	74%	43%	CBE	CBE
4	Amplitude	0.04	0.186	0.322	0.612	CBE	CBE
	Phase	-0.15π	1.503π	0.281π	1.53π	CBE	CBE
	Relative error	102%	86.5%	35.8%	24.8%	CBE	CBE
8	Amplitude	0.058	0.144	0.413	0.558	CBE	CBE
	Phase	0.176π	1.508π	0.292π	1.517π	CBE	CBE
	Relative error	50.7%	44%	17.4%	13%	CBE	CBE
16	Amplitude	0.0784	0.122	0.457	0.529	CBE	CBE
	Phase	0.252π	1.506π	0.296π	1.509π	CBE	CBE
	Relative error	25.3%	22.2%	8.6%	6.7%	CBE	CBE

[a]CBE: cannot be encoded.

was not considered because its realization requires a 4×4 pixelated structure within each pixel rather than continuous structures, and thus fabrication efforts are significantly increased. Nevertheless, it should be mentioned that, with proper fabrication procedures, the improved 2-D structure yields very good results.

Comparing Tables 1–3 makes it evident that the proposed approach is superior compared with the other approaches. The comparison should concentrate primarily on the case of low-amplitude levels when much of the signal's energy needs to be diffracted out of the region of interest, which is defined as the zero-order window. On the other hand, for the case of high amplitude with a value close to 1 the performances of the present approach and the one described by Ref. 19 coincide because for such a case $\phi^1 = \phi^2$, and thus the partition within the macropixel disappears. In such a case, no phase error occurs, and the sinc envelope is the only reason for amplitude error. On the other hand, it was shown in Ref. 17 that, for the fixed-phase-level approach, one cannot achieve an amplitude with unity value for any phase level. As a result of that outcome, the maximum amplitude should be set at a value of 1/2, thus limiting the light efficiency to no more than 25%. That approach requires higher spatial resolution, on one hand, but needs only two constant etching steps on the other hand.

5. Computer Simulations

To estimate the performance of the proposed approach, we carried out several computer simulations. The simulations were based on a 2-D filter structure with macropixels of 7×7 cells ($\delta\nu = 7_{\text{subpixels}}$) so that $\delta\nu/\sqrt{2} \approx 5_{\text{subpixels}}$. The reconstruction quality can be estimated by use of the mean-squared error (MSE) criterion, defined as

$$\text{MSE} = \sum_n \sum_m |h_{n,m}^{\text{desired}} - h_{n,m}^{\text{obtained}}|^2, \tag{20}$$

where $h_{n,m}$ is the field at the pixel (n, m), namely, its phase and amplitude.

To evaluate the error requires that the intensity of both the desired and the obtained fields be normalized in accord with

$$\sum_n \sum_m |h_{n,m}^{\text{desired}}|^2 = \sum_n \sum_m |h_{n,m}^{\text{obtained}}|^2 = 1. \tag{21}$$

In Eq. (21) the summation is over the region of interest of the zero-padded image, namely, the original image.

The simulations involved an image, which was chosen to be the letter H, as shown in Fig. 4(a). This image contains only amplitude data, namely, ones and zeros. The original image contained 32×32 macropixels, but with a padding factor of $P = 4$ it ended up as a matrix of 128×128 macropixels. The amplitude of the reconstructed image with a corresponding MSE value of 0.193 is displayed in Fig. 4(b). In addition to the MSE, one should also evaluate the

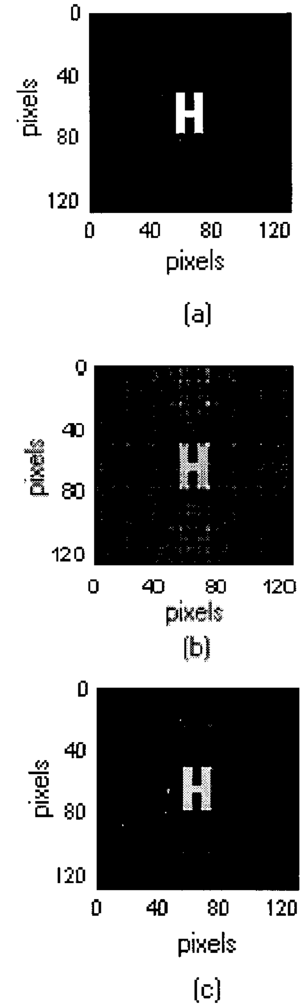

Fig. 4. Effect of zero padding on the quality of the reconstructed image of the letter H: (a) desired reconstruction, (b) reconstructed image for the case of $P = 4$, (c) reconstructed image for the case of $P = 8$.

light efficiency of the filter. The proposed method is based on a phase-only encoding method with zero attenuation. Because the desired amplitude of the original image may be less than 1, the filter should exhibit finite attenuation, meaning that a finite percentage of the light's intensity needs to be diverted outside the region of interest. The power of the original filter that one needs to generate is

$$I^{\text{desired}} = \sum_n \sum_m |A_{n,m}|^2, \tag{22}$$

where $A_{n,m}$ is the normalized amplitude of the Fourier transform of the desired reconstruction. Denoting the number of pixels in each axis as Δ means that the total power impinging upon the filter is the sum of the intensities of each and every pixel, resulting in

$$I = \sum_k \sum_p |A_{k,p}^{\text{filter}}|^2 = \sum_k \sum_p |1|^2 = \Delta^2. \tag{23}$$

Let's define ρ_{desired} as the ratio of the intensity in the region of interest (where the zero-order recon-

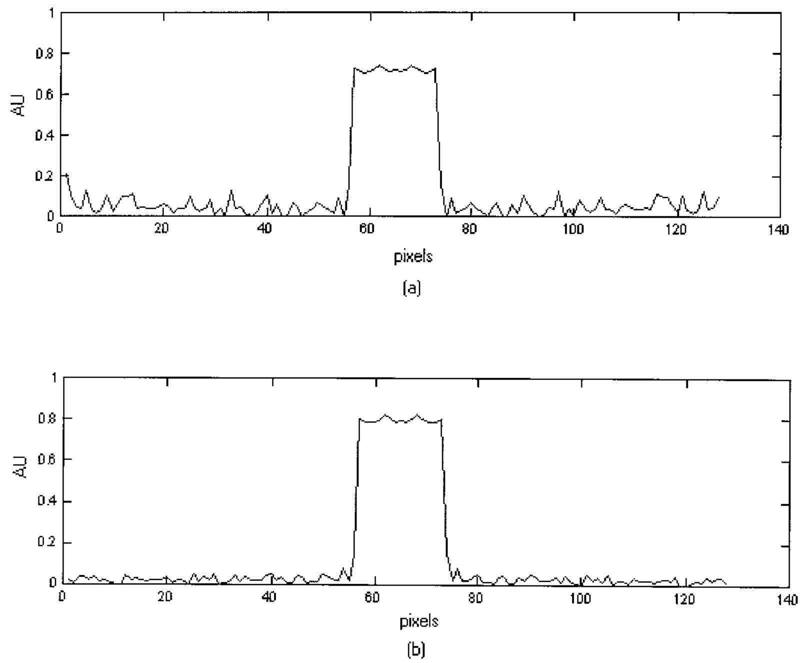

Fig. 5. Cross section of the reconstructed image [Figs. 4(a) and 4(b), respectively] through the center axis: (a) $P = 4$, (b) $P = 8$.

structed image is located) with respect to the total illumination intensity:

$$\rho_{\text{desired}} = \frac{\sum_n \sum_m |A_{n,m}^{\text{desired}}|^2}{\Delta^2}. \tag{24}$$

The filter $H(\nu_x, \nu_y)$ should diffract the unwanted power to higher orders so that $\rho_{\text{obtained}}/\rho_{\text{desired}}$ is as close as possible to unity. We thus define an efficiency parameter η as

$$\eta = \frac{\rho_{\text{obtained}}}{\rho_{\text{desired}}}, \tag{25}$$

where

$$I_{\text{zero order}}^{\text{obtained}} \rho_{\text{obtained}} = \frac{I_{\text{zero order}}^{\text{obtained}}}{I_{\text{total}}^{\text{obtained}}}$$

is the power contained in the zero-order reconstructed zero-padded image and $I_{\text{total}}^{\text{obtained}}$ is the total power of all the diffraction orders of the reconstructed image. The efficiency parameter η allows us to estimate the quality of the power distribution over the zero order relative to the intensities of other diffraction orders of the reconstructed image. In the simulation discussed the efficiency obtained is $\eta = 2.01$, which implies that we have received, in the region of interest, twice the desired intensity we would have obtained, should the hologram be ideal. This result implies that the encoding method could not diffract all the undesired light toward higher orders.

To verify the advantage of padding the original image with zeros, we carried out a similar simulation, this time with $P = 8$. In this case, as can be seen from Fig. 4(c), the performance was considerably enhanced in comparison with the $P = 4$ case shown in Fig. 4(b). The reconstruction is quantitatively described by MSE = 0.113 and $\eta = 1.57$. Cross sections for these cases are shown in Figs. 5(a) and 5(b), respectively.

To take into consideration the stringent manufacturing constraints and difficulties, we considered phase quantization as well. The results for 32 phase levels with $P = 4$ are shown in Fig. 6. Fewer quantization levels as a result of the sensitivity of the hologram to dc power results in a lesser performance. The encoding of amplitude information by a phase-

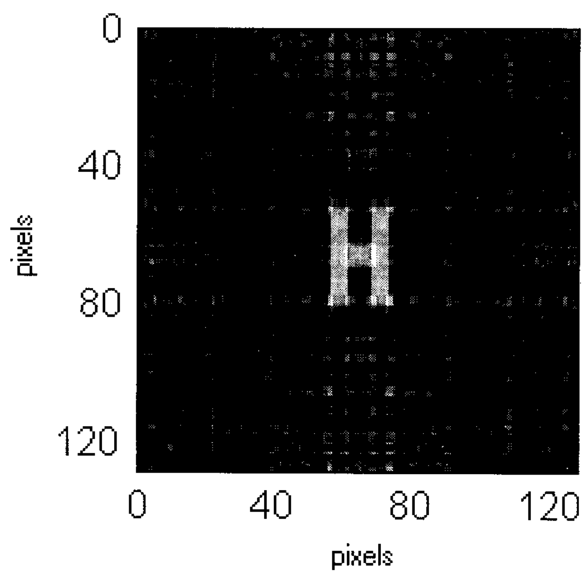

Fig. 6. Quantization effect on image quality. The simulation was done for the $P = 4$ case [Fig. 4(a)] with 32 phase levels.

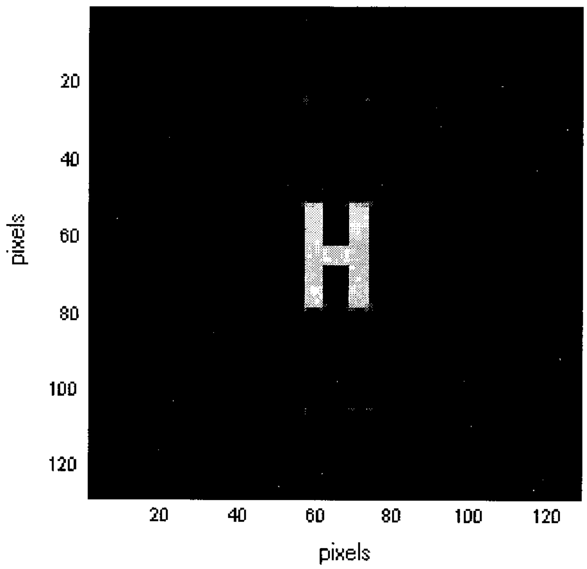

Fig. 7. Image quality for the case of the desired construction's being multiplied by a quadratic phase. The simulation was carried out for $P = 4$.

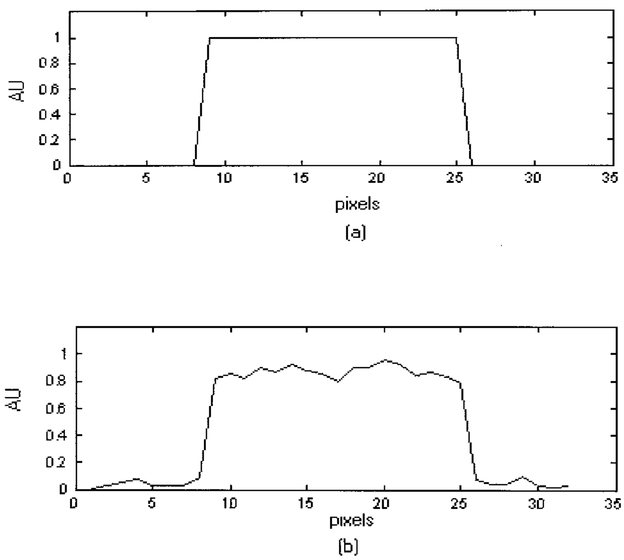

Fig. 8. Intensity variations along the central cross section shown in Fig. 7: (a) the desired reconstruction, (b) the simulation results.

only filter involves diffracting the undesired light toward off-axis diffraction orders. On the other hand, if one desires to reconstruct a constant phase distribution, the central Fourier coefficient is relatively large, whereas higher-frequency coefficients are relatively low. For such a case, significant amplitude modulation has to be achieved by use of a phase-only filter, and such a case is very demanding, leading to unavoidable errors. Therefore it would be much better to obtain a Fourier transform of an object in which the amplitude variations are significantly reduced.

A common approach for achieving the above task is to multiply the object by a random phase, similar to the use of a ground glass in holographic applications. Unfortunately, the reconstruction achieved by this approach is highly degraded owing to speckle effects. Thus we decided to multiply the reconstructed object by a quadratic phase, which is equivalent to one's decoding the image with a Fresnel transform instead of a Fourier transform. This case leads to a uniform energy distribution along the Fourier plane. The curvature of the quadratic phase should be such that the phase difference between two adjoining pixels of the reconstructed object cannot exceed, say, $\pi/4$. Applying this approach to the letter H under consideration, we multiplied it by a quadratic phase in accord with

$$\phi_{n,m} = 4\pi\left[1 - \frac{(n - n_0)^2 + (m - m_0)^2}{{n_0}^2 + {m_0}^2}\right], \tag{26}$$

where (n_0, m_0) are the coordinates of the center of the image. In addition, 16 phase levels and a zero-padding ratio of $P = 4$ were used. The simulated reconstruction is shown in Fig. 7. A trace of the intensity along the central cross section of the image is given in Fig. 8. The reconstructed image can avoid the addition of the quadratic phase to the original image if one performs an inverse Fresnel transform instead of an inverse Fourier transform.

6. Experimental Results

For verifying the quality and the validity of this encoding method an optical experiment was carried out. The object chosen for optical reconstruction was,

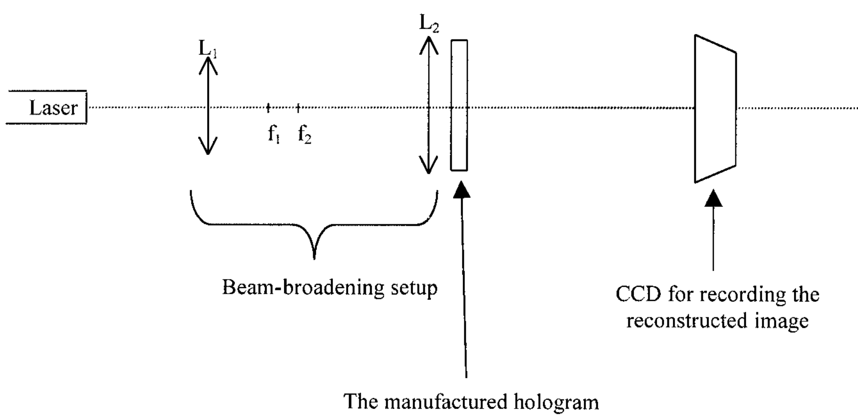

Fig. 9. Optical experimental setup: f_1 and f_2 are the focal lengths of L_1 and L_2, respectively.

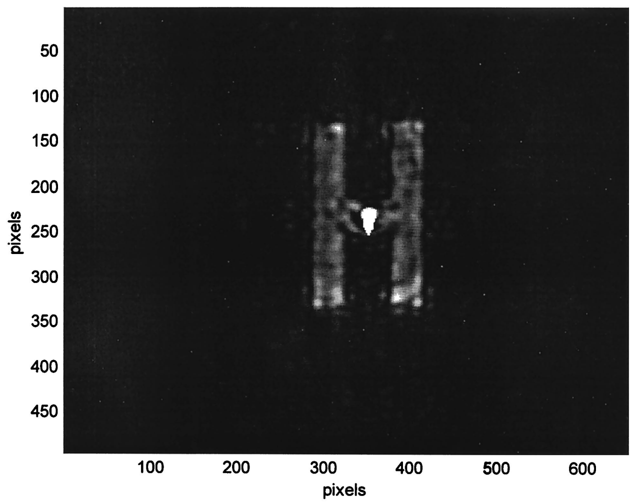

Fig. 10. Obtained optical reconstruction from the setup shown in Fig. 9.

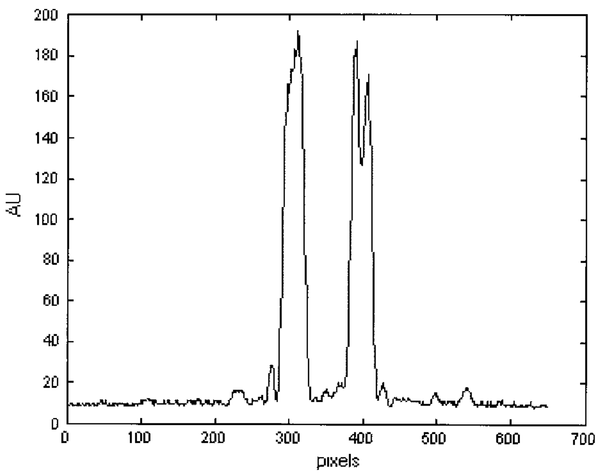

Fig. 11. Intensity variations along the horizontal cross section shown in Fig. 10.

again, the letter H. Sixteen phase levels, $P = 4$, and quadratic phase multiplication were used. The lateral dimensions of each macropixel were chosen to be 70 μm, and thus the filter size was 1.2 cm. Reconstruction was achieved by a standard Fourier setup, as shown in Fig. 9. A He–Ne laser ($\lambda = 632.8$ nm) and an 8-bit CCD camera were used. The zero-order region of the reconstructed image, presented in Fig. 10, was distributed over 200×200 CCD pixels, which is equivalent to the distribution needed for lateral dimensions of 2×2 mm. An example of a horizontal cross section is given in Fig. 11. Because a Fourier-type CGH was used, the dc component is very sensitive to fabrication errors (see the figure). This sensitivity is the reason for the strong, undesired dc peak. Improved monitoring of the etching process should significantly reduce this problem. Alternatively, near-field rather than far-field reconstruction can be used.

7. Conclusions

A new implementation of a zero-order (on-axis) CGH, which permits the encoding of a phase as well as an amplitude by use of a phase-only filter, has been suggested. The proposed approach is based on the fixed, centrosymmetric spatial partitioning of each pixel into two subregions. Each subregion is represented by a different phase value (a different etching level). Such an approach can easily be implemented with common micro-optics fabrication techniques. The encoding method has been described by use of a detailed mathematical analysis, and the necessary approximations, which cause some reconstruction errors, have been pointed out.

The description of the proposed approach has been followed by a comprehensive error discussion, including a comparison with different approaches. The comparison results, which were based on our estimating the error terms of these approaches, emphasized the improved performance of the suggested approach. Several computer simulations were carried out that took into account phase quantization and different padding ratios. We have also experimented with such an element so that practical limitations could be faced. The optical reconstruction was satisfactory except for a dc peak that was caused by manufacturing inaccuracies. Optical elements that are implemented by use of the suggested approach can be used for a variety of applications such as optical correlators, displays, and beam-shaping devices.

References

1. R. Gruhlke, L. Giamonna, C. Langhorn, K. Kanzler, and J. Kedmi, "Medical and industrial laser beam shaping by diffractive optical elements," in *Laser Coherence Control: Technology and Applications*, T. K. Kessler and H. T. Powell, eds., Proc. SPIE **1870,** 120–129 (1993).
2. J. L. Horner and J. R. Leger, "Pattern recognition with binary phase-only filter," Appl. Opt. **24,** 609–611 (1985).
3. S. J. Walker and J. Jahns, "Optical clock distribution using integrated free-space optics," Opt. Commun. **90,** 359–371 (1992).
4. T. R. M. Sales and G. M. Morris, "Diffractive–refractive behavior of kinoform lenses," Appl. Opt. **36,** 253–257 (1997).
5. B. R. Brown and A. W. Lohmann, "Complex spatial filtering with binary masks," Appl. Opt. **5,** 967–969 (1966).
6. A. W. Lohmann and D. P. Paris, "Binary Fraunhofer holograms generated by computer," Appl. Opt. **6,** 1739–1749 (1967).
7. W. H. Lee, "Sampled Fourier transform holograms generated by computer," Appl. Opt. **9,** 639–643 (1970).
8. C. B. Burkhardt, "A simplification of Lee's method of generating holograms by computer," Appl. Opt. **9,** 1949 (1970).
9. C. K. Hsueh and A. A. Sawchuck, "Computer-generated double-phase holograms," Appl. Opt. **17,** 3874–3883 (1978).
10. N. C. Gallagher and J. A. Bucklew, "Nondetour phase digital holograms: an analysis: an errata," Appl. Opt. **19,** 4266–4272 (1980).
11. R. M. Matic and E. W. Hensen, "Nondetour computer-generated holograms: an improvement variation," Appl. Opt. **21,** 2304–2305 (1982).

12. W. H. Lee, "Computer-generated holograms: techniques and applications," in *Progress in Optics*, 16th ed., E. Wolf, ed. (North-Holland, Amsterdam, 1978), pp. 121–232.
13. U. Levy, E. Marom, and D. Mendlovic, "Modifications of detour phase computer-generated holograms," Appl. Opt. **37,** 3044–3052 (1998).
14. J. P. Kirk and A. L. Joens, "Phase-only complex-valued spatial filter," J. Opt. Soc. Am. **61,** 1024–1028 (1971).
15. J. Turunen, P. Vahimaa, M. Honkanen, O. Salminen, and E. Noponen, "Zeroth-order complex-amplitude modulation with dielectric Fourier-type diffractive elements," J. Mod. Opt. **43,** 1389–1398 (1996).
16. Y. Danziger, E. Hasman, A. A. Friesem, and A. W. Lohmann, "Multilevel diffractive elements for generalized wave-front shaping," Opt. Eng. **35,** 2556–2565 (1996).
17. U. Levy, D. Mendlovic, and Z. Zalevsky, "On-axis phase-only computer-generated holograms based on a minimal etching process," J. Mod. Opt. **45,** 1437–1449 (1998).
18. J. M. Florence and R. D. Juday, "Full complex spatial filtering with a phase-mostly DMD," in *Wave Propagation and Scattering in Varied Media II*, V. K. Varadan, ed., Proc. SPIE **1558,** 487–498 (1991).
19. D. Mendlovic, G. Shabtay, U. Levy, Z. Zalevsky, and E. Marom, "Encoding technique for design of zero-order (on-axis) Fraunhofer computer-generated holograms," Appl. Opt. **36,** 8427–8434 (1997).